Geophysical Research Letters

RESEARCH LETTER
10.1029/2023GL106668

Key Points:

- REPT PHA data can be used to produce high energy resolution flux spectra of >1 MeV electrons
- Electron penetrations below $L = 2$ during strong geomagnetic storms extend in energy up to 1.3 MeV
- Electron penetrations below $L = 2$ at energies 1–1.3 MeV are associated with butterfly pitch angle distributions

Supporting Information:

Supporting Information may be found in the online version of this article.

Correspondence to:

D. O'Brien,
declan.obrien@lasp.colorado.edu

Citation:

O'Brien, D., Li, X., Khoo, L., Selesnick, R. S., Hogan, B., Zhao, H., et al. (2024). Observations of relativistic electron enhancement and butterfly pitch angle distributions at low L (<3). *Geophysical Research Letters*, *51*, e2023GL106668. https://doi.org/10.1029/2023GL106668

Received 5 OCT 2023
Accepted 12 DEC 2023

Author Contributions:

Conceptualization: D. O'Brien, X. Li
Formal analysis: D. O'Brien
Funding acquisition: X. Li
Investigation: D. O'Brien
Methodology: D. O'Brien, X. Li, L. Khoo, R. S. Selesnick
Project Administration: X. Li
Software: D. O'Brien, L. Khoo, V. Hoxie
Supervision: X. Li
Validation: D. O'Brien, R. S. Selesnick, H. Zhao, V. Hoxie
Visualization: D. O'Brien
Writing – original draft: D. O'Brien
Writing – review & editing: X. Li, L. Khoo, R. S. Selesnick, B. Hogan, H. Zhao, Y. Mei, V. Hoxie, D. N. Baker, S. G. Kanekal

Observations of Relativistic Electron Enhancement and Butterfly Pitch Angle Distributions at Low L (<3)

D. O'Brien[1,2], X. Li[1,2], L. Khoo[3], R. S. Selesnick[4], B. Hogan[1,2], H. Zhao[5], Y. Mei[1,2], V. Hoxie[1], D. N. Baker[1,2], and S. G. Kanekal[6]

[1]Laboratory for Atmospheric and Space Physics, University of Colorado Boulder, Boulder, CO, USA, [2]Department of Aerospace Engineering Sciences, University of Colorado Boulder, Boulder, CO, USA, [3]Department of Astrophysical Sciences, Princeton University, Princeton, NJ, USA, [4]Space Vehicles Directorate, Air Force Research Laboratory, Albuquerque, NM, USA, [5]Physics Department, Auburn University, Auburn, AL, USA, [6]NASA Goddard Space Flight Center, Greenbelt, MD, USA

Abstract Electrons in Earth's outer radiation belt are highly dynamic, with fluxes changing by up to orders of magnitude. The penetration of electrons from the outer belt to the inner belt is one such change observed during geomagnetic storms and was previously observed in electrons up to 1 MeV for some strong storms observed by the Van Allen Probes. We analyze pulse height analysis data from the Relativistic Electric and Proton Telescope (REPT) on the Van Allen Probes to produce electron flux measurements with lower minimum energy and significantly improved resolution compared to the standard REPT data and show that electron penetrations into the inner belt ($L \leq 2$) extend to at least 1.3 MeV and penetrations into the slot region ($2 < L < 2.8$) extend to at least 1.5 MeV during certain geomagnetic storms. We also demonstrate that these penetrations are associated with butterfly pitch angle distributions from 1 to 1.3 MeV.

Plain Language Summary Electrons in Earth's outer radiation belt are highly dynamic with the amount and energy of them changing drastically, especially during geomagnetic storms. The penetration of electrons from the outer belt to the inner radiation belt is one such change and was previously observed in electrons with energies ≤1 MeV during some of the strongest storms during the Van Allen Probes mission. Electrons in the radiation belts also have a pitch angle that describes what portion of their motion is along or perpendicular to the direction of the magnetic field. Pitch angle distributions (PAD) are often used to gain information on the dynamics of the electrons, as unstable distributions can be caused by and indicative of wave activity that cannot always be measured directly. PADs with a minimum at 90°, called butterfly PADs, are one such unstable distribution that have previously been observed in penetrating electrons with energies ∼100–900 keV. We use instrument simulation to analyze data from the Van Allen Probes that could not previously be analyzed to show that the maximum energy of these penetrations is higher than previously observed, up to 1.3 MeV, and that these penetrations are associated with butterfly PADs at 1–1.3 MeV.

1. Introduction

Earth's inner magnetosphere contains regions of trapped, high-energy electrons and protons that form two, roughly toroidal belts called the radiation belts. The inner radiation belt extends from $L \leq 2$ to the top of the atmosphere near the equator, the outer belt extends from $L = 3$–6, and, during quiet times, there is a low flux region between the two belts called the slot region. Under quiet-time conditions, the inner belt electron populations have energies of 10–100s keV while significant fluxes up to a few MeV are observed in the outer belt (e.g., Claudepierre et al., 2019). During and after geomagnetic storms, electron flux enhancements due to penetration from the outer belt can be observed in the inner belt and slot region (e.g., Li et al., 2019; Selesnick, 2015; Zheng et al., 2006). These are commonly observed up to several hundred keV (Claudepierre et al., 2017; Zhao et al., 2023) but are much less common at higher energies. Previous observations have shown similar enhancements at energies as high as 1 MeV (Claudepierre et al., 2019) during a few strong geomagnetic storms, but the low flux of these populations combined with the large amount of background flux from high energy protons being detected as electrons (Li et al., 2015) within the slot region and inner belt makes it difficult to tell whether any higher energy enhancements have occurred during the Van Allan Probes era (2012–2019). The question therefore remains unanswered: what are the highest energy electrons that can exist in the inner belt ($L \leq 2$)?

While spin-averaged fluxes provide a great deal of information (e.g., Li et al., 2009) about electron populations, pitch angle distributions show a fuller picture of the electrons (e.g., Li et al., 2022; Yu et al., 2016). Charged particles within magnetic fields gyrate around magnetic field lines. Generally, some portion of the motion is parallel to the field line and some portion is perpendicular to it, and the angle of the velocity vector with respect to the field line is called the pitch angle of the particle. Within the roughly dipolar fields of Earth's inner magnetosphere, the motion of particles along field lines brings them to higher magnetic field strengths at lower altitudes. The increasing field strength increases the pitch angle of the particle until it reaches 90° and the particle reverses direction. This motion is referred to as bounce motion and the point at which the bounce occurs is called the mirror point. Near the magnetic equator, particles with pitch angles below some limit will have mirror points that are within the planet's atmosphere. These particles are considered lost within one bounce period due to collisions with the neutral atmosphere, so this pitch angle limit is called the loss cone. Due to wave-particle interactions (WPI) within magnetospheres, particle pitch angles tend to change in a random walk (Roberts, 1969). Because of this process, combined with the loss cone, particle populations most commonly have pitch angle distributions with a maximum at 90° and a roughly sine distribution to low flux near the edge of the loss cone (Zhao et al., 2018). Several previous studies (e.g., Hua et al., 2019; Zhao et al., 2014a, 2014b) have used in-situ measurements and modeling to investigate the PADs associated with 100s keV electrons in the slot region and inner belt. Zhao et al. (2014b), using data from MagEIS instrument on the Van Allen Probes, reported observations of the formation of pitch angles with minima at 90°, referred to as a butterfly PAD, at up to 593 keV in the slot region and inner belt after geomagnetic storms concurrent with flux enhancements. These butterfly PADs remained in the slot region for days and were, for some energies, persistent within the inner belt. Hua et al. (2019), also using MagEIS data, extended this maximum energy up to 899 keV and used diffusion modeling to argue that these butterfly PADs could be forming at $L > 2.8$ and then radially diffusing inward, though for the model to match the observations, the radial diffusion coefficients used, DLL (Ozeke) (Ozeke et al., 2014), had to be enhanced by a factor of 5. For the March and June 2015 storms, where Claudepierre et al. (2019) showed 1 MeV flux enhancement, Li, Bortnik, et al. (2016) reported observations of the formation of butterfly PADs at the inner edge of the outer belt ($L = 2.7$–3.6) from 75 keV to 5.2 MeV and used the effects of magnetosonic waves in a diffusion model to recreate their formation. In contrast, Albert et al. (2016) used a diffusion model without magnetosonic wave effects to demonstrate that these butterfly PADs could form at $L = 2$ without magnetosonic waves present. The difference in this case was that the model used was a 2-dimensional diffusion model that models both momentum and pitch angle and accounts for the relationship between the two with the cross term, which couples the diffusion in momentum and pitch angle.

In this paper, we show that the REPT PHA data, combined with the standard data of REPT and MagEIS (see next section), enable us to produce high resolution energy spectra of electrons in the inner belt and slot region and to address the question of the highest energy electrons in the inner belt and slot region and characterize the PADs in detail.

2. Instrument Simulation and Use of PHA Data

This work makes use of the data from both the Magnetic Electron Ion Spectrometer (MagEIS, Blake et al., 2013) and Relativistic Electron and Proton Telescope (REPT, Baker et al., 2013) instruments onboard the Van Allen Probes (Mauk et al., 2013), two identical satellites with elliptical, following orbits that give coverage of both radiation belts, to investigate the behavior of electrons with energies 1 MeV and greater during strong storms. In addition, simulation in Geant4 has allowed for the use of REPT pulse height analysis (PHA) data to produce high resolution electron energy spectra with lower flux background due to high energy protons (Agostinelli et al., 2003; Allison et al., 2006, 2016). The level 3 REPT flux data (referred to hereafter as REPT L3) has a minimum energy (1.8 MeV) significantly higher than the highest energy (∼1 MeV) flux enhancement observations recorded by MagEIS (Claudepierre et al., 2019) and contamination from penetrating protons makes it unable to provide reliable observations below L of ∼2.6 (Baker et al., 2021; Claudepierre et al., 2019; Li et al., 2015). This study therefore makes use of the REPT PHA data, individual event data that provides the energy deposited on each of REPT's nine detectors by individual particles. In the standard REPT operating mode, each electron event would be binned into one of 12 energy channels, the behavior of which have been characterized through simulation and electron and proton beam tests (Baker et al., 2021). With the PHA data set available, a new binning process is formulated and analyzed using Monte Carlo simulations in the Geant4 toolkit to characterize the behavior of new electron bins. The result of this process is an instrument response function that quantifies the

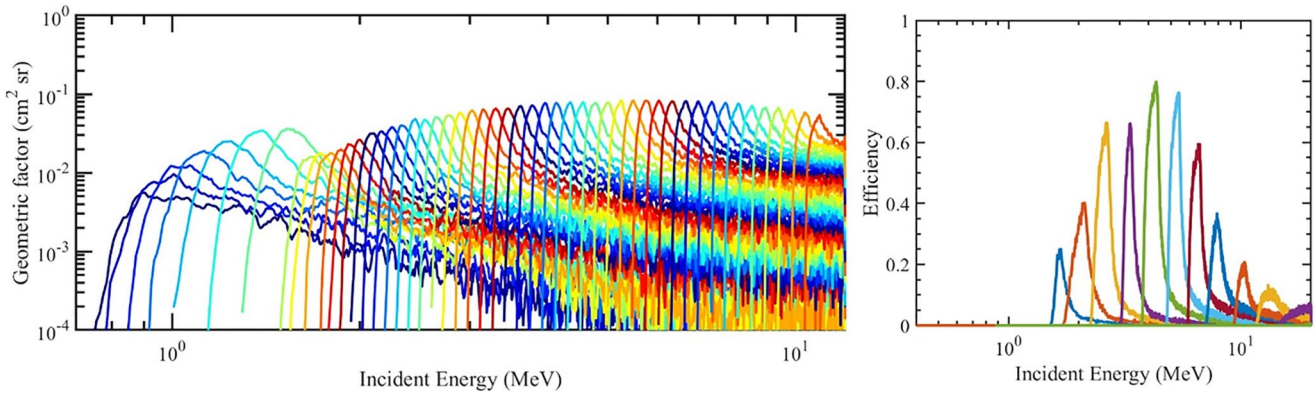

Figure 1. REPT electron channel responses. The left figure shows the simulated response to an isotropic source of the newly defined electron channels. Each curve corresponds to one energy channel. The right figure is provided as a point of comparison and is the simulated boresight efficiency of the same simulated instrument to the original 12 REPT electron channels. Note that the *y* axes have different scales.

contribution of electrons at each energy to each channel (e.g., Khoo et al., 2022). A similar process was previously used for proton detection from REPT PHA data (Selesnick et al., 2018) and to constrain the electron flux at low L at the energies of the standard REPT data (Li et al., 2015). By including events that triggered only the first detector, which are excluded in the processing of the L3 data, these channels extend to lower energy and, with the updated simulation, expand to more channels with a higher energy resolution than the original 12 channels; the response function for these new channels is compared to the response function of the original channels in Figure 1. Figure 1 shows the response of each of the sets of channels to electrons entering the instrument from within the field of view (FOV). These channels nominally measure electrons but also receive counts from high energy protons that deposit similar amounts of energy on the detectors (Li et al., 2015). This proton contamination is present in some amount in all of the REPT L3, MagEIS L3, and the REPT PHA data collected in regions with significant high energy proton fluxes (generally $L < 2.6$) but is less significant in the REPT data than the MagEIS data due to REPT's larger geometric factor. The PHA data has a cadence of 0.012 s, storing one event each time; this means that the available PHA data is only a subset of the total event set that is used to produce the binned count rate measurements used to produce L3 data. To account for this, the PHA-based binned count rates must be averaged over relatively long time periods, dependent on the flux, in order to get statistically significant results and then normalized to the detector 1 count rate (Selesnick et al., 2014). Once these count rates are calculated they are then converted to fluxes.

The response of an instrument to a given flux spectrum can be found by integrating the effects on all channels, as governed by the response function, with the flux. Because of this, finding the flux from the count rates is an inverse problem for which a unique solution cannot be found. The method used to calculate the flux for the original REPT electron channels is the Bowtie method (Baker et al., 2021; Selesnick & Blake, 2000) which provides one flux estimate per channel at an estimated energy centroid with some channel width and efficiency by assuming some shape of the flux spectrum (frequently an exponential function). In order to lower the minimum energy that is effectively measured, this study instead makes use of a least squares method (Tarantola, 2005; Tarantola & Valette, 1982). In this method, here adapted from Khoo et al. (2022) and Selesnick et al. (2018), the contribution of particles of each energy to the count rate of each channel, which is useful due to random electron scattering and range straggling (Bischel, 1988), is considered and a statistical fit of the most likely flux spectrum is found by iteratively minimizing the least squares criterion. This method produces more accurate flux spectra than the Bowtie method because it considers the entire detailed response function and allows for flux spectra that are continuous with an energy resolution limited by a smoothing factor which is discussed further in the Supporting Information S1. This method is applied to both spin-averaged fluxes and pitch-angle-binned fluxes. The net effect of using the PHA data and the least squares method is a flux spectrum with a lower minimum energy and much improved energy resolution compared to the standard REPT electron channels. Because of the reduced sampling rate, time averages of at least a day are required to achieve statistically significant results for the 0.2 wide L bins used in this study. The least squares method also gives the flux spectrum a calculated uncertainty, which is helpful especially in low flux regions.

In order to compare to the PHA data and extend the analysis to lower energy, PAD and spin-averaged flux spectra are also produced using standard MagEIS and REPT data. The spin-averaged fluxes are obtained by taking the MagEIS L3 corrected and REPT L3 fluxes and averaging them over both spacecraft spin and L range. MagEIS fluxes are already binned into one of 11 local pitch angle bins. REPT L3 and PHA data are binned here to the same bins to match the MagEIS data. All local pitch angles are used to calculate their equivalent equatorial pitch angles using a dipolar field model.

3. Results

The spin-averaged PHA fluxes provide measurements of 1.1–7 MeV electrons. These measurements have lower background due to proton contamination at $L < 3$ than MagEIS due to REPT's larger geometric factor and have better resolution and a lower minimum energy than the RPET L3 flux. Like the best estimates of 1 MeV electron flux enhancements using MagEIS from Claudepierre et al. (2019), spin-averaged flux spectra from REPT PHA are averaged from both Van Allen Probes for L ranges representing the inner belt (1.8–2.0), slot region (2.4–2.6), and inner edge of the outer belt (2.8–3.0) for the 5 days before and 5 days after the day containing the Dst minimum of the strong June 2015 (min Dst −198 nT) and September 2017 (min Dst −122 nT) geomagnetic storms. These storms are selected due to measurement by Claudepierre et al. (2019) of flux enhancement of up to 1 MeV electrons during them. The results of this are presented along with MagEIS (background corrected) and REPT L3 fluxes averaged for the same time periods and L ranges for both Van Allen Probes in Figure 2. In order to highlight the change in flux, the REPT PHA flux spectra from before and after the September 2017 storm are directly compared in Figure 3. A few points are worth noting within these results:

1. After both magnetic storms, electron flux enhancements up to 3 MeV are observed at the inner edge of the outer belt ($2.8 < L < 3$) in all three data sets (MagEIS High, REPT L3, and REPT PHA).
2. The REPT L3 flux (1.8 MeV and above) shows no change in measured flux from before to after either storm in the slot region ($2.4 < L < 2.6$) or inner belt ($1.8 < L < 2$), which suggests that the measured fluxes do not represent electrons but, more likely, contamination from inner belt protons (Li et al., 2015).
3. The REPT PHA results show electron flux enhancements of 1.1–1.3 MeV after the storms all the way down to $L = 1.8$ that align spatially and temporally within the inner belt with those shown by MagEIS at 1 MeV; no change was observable for MagEIS High at its next channel (1.5 MeV). Overall, we can state that no measurable enhancements are observed for >1.3 MeV electrons in this region ($1.8 < L < 2$).
4. In the slot region, a greater than an order of magnitude enhancement of electrons at ∼1.3 MeV was seen in the REPT PHA data. Similar enhancement at 1 MeV was also seen in MagEIS High data, but no change is seen at 1.5 MeV in the MagEIS High data. Significant enhancements up to ∼1.5 MeV are also discernible at the REPT PHA data, particularly in the June 2015 storm. This result and the enhancements in the outer belt are consistent with the early Van Allen Probes result from Baker et al. (2014) establishing the "impenetrable barrier" at $L = 2.8$ for ultra-relativistic electrons.
5. Back to the inner edge of the outer belt ($2.8 < L < 3$), the dynamic behaviors 4–6 MeV electron fluxes were well captured by both the REPT PHA and the REPT L3 data: a decrease for these ultra-high energy electrons after the June 2015 storm and an increase after the September storm. The differing behaviors between the two storms are likely due to the different preconditions, which are most obvious in the order of magnitude higher ultra-high energy electron flux prior to the June 2015 storm. After both storms, the flux spectra look quite similar with a roughly exponential shape, extending to at least 6 MeV. For the June storm, there were flux dropouts (e.g., Hogan et al., 2021) at these ultra-high energies along with broad spectrum enhancement in lower energies, while only enhancement is observable in the September 2017 storm for these ultra-high energies along with broad spectrum enhancements.

In order to further investigate the behavior of 1–1.8 MeV electrons at $L < 2.6$, MagEIS and REPT PHA data can be binned by pitch angle to produce PADs. Using the 11 pitch angle bins defined by the MagEIS L3 data, Figure 4 shows the equatorial pitch angle distributions of electrons at these energies lower in the slot region and in the inner belt for the September 2017 storm. This shows that flux enhancement and butterfly PADs are observed up to 1.75 MeV at $L = 2.4$–2.6. At even lower L (<2.2), butterfly PADs and flux enhancement are observed at 1.15 MeV down to $L = 1.8$ and 1.35 MeV at $L = 2$–2.2. Even though a butterfly PAD is not apparent in the $1.8 < L < 2$ PAD fluxes for 1.35 MeV, taking the difference of the flux before and after the storm,

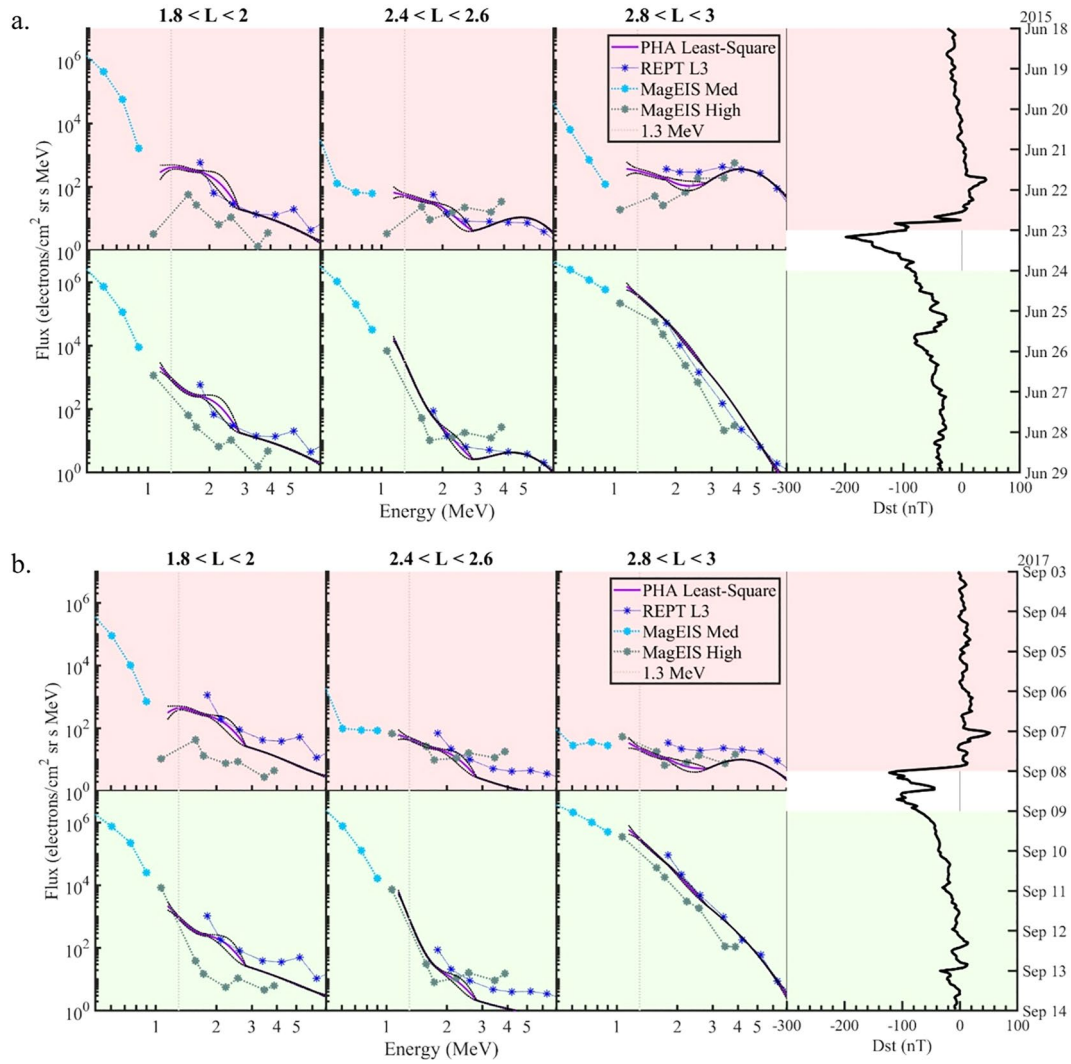

Figure 2. Flux energy spectra comparisons from PHA data using the nonlinear least-square method (purple), corrected fluxes from MagEIS High (gray) and Med (cyan), and from the REPT L3 data (blue). All fluxes are spin-averaged 5 days averages averaged over both of the Van Allen Probes. The fluxes shown are for the 5 days before (red/top panels) and 5 days after (green/bottom panels) (a). The strong June 2015 geomagnetic storm and (b). The September 2017 geomagnetic storm. The Dst index for the times averaged over are shown in the right-side panel. The black dotted lines represent the uncertainty of the determined PHA fluxes and bulge between about 2 and 2.5 MeV, which also represents an uncertainty, is due to the combining of range 1+, where only detector 1 is triggered, and range 2+, where only detector 1 and detector 2 are triggered, fluxes in this energy range.

shown in the bottom row Figure 4, reveals that the change in flux at this energy does have a 90° minimum and a similar shape to a butterfly PAD. Additionally, this shows a clearer butterfly PAD at 1.35–1.55 MeV in the slot region.

4. Discussion and Conclusion

Previous results from Claudepierre et al. (2019) showed flux enhancements up to 1 MeV in the inner belt for the same two storms for which observations are shown in Figure 2. The energy channels for MagEIS go from a nominal energy of 1.01–1.54 MeV and these enhancements are shown in the 1.01 MeV channel but not the 1.54 MeV channel. The REPT PHA data reproduce the existence of these enhancements at 1 MeV and extend to a higher energy, ~1.3 MeV. This also shows that the exponential energy spectrum of these penetrations continues to a higher energy than previously demonstrated, but any potential enhancement at higher energy is below the

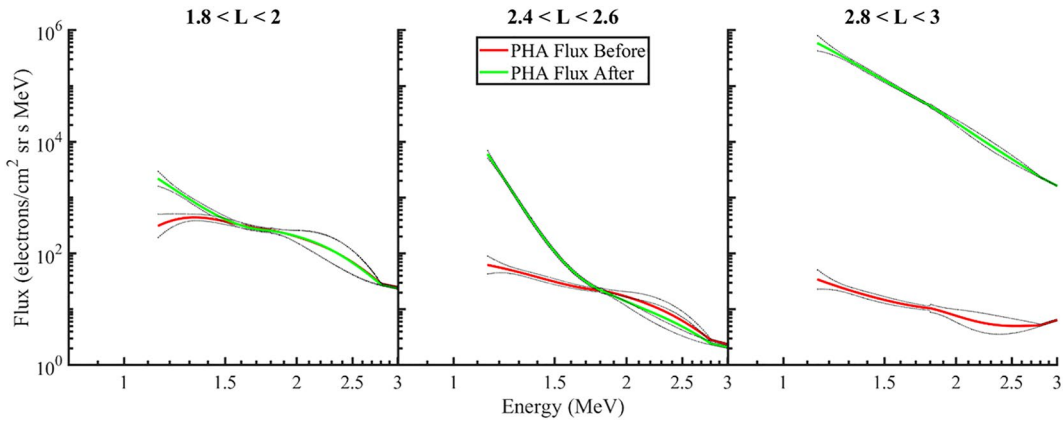

Figure 3. Direct comparison of the REPT PHA flux spectra for the 5 days before (green) and after (red) the September 2017 storm for the same 3 L ranges shown in Figure 2. These spectra are the same spectra shown in Figure 2 as PHA Least-Square.

background level of the PHA flux data at 1.5 MeV as well. Additionally, the associated butterfly PADs have not previously been observed at or above 1 MeV within the slot region or inner belt ($L < 2.6$). Given previous observations at lower energies (e.g., Zhao et al., 2014a, 2014b) along with the observed formation of butterfly PADs at higher energies near the inner edge of the outer belt for similarly strong storms (Li, Bortnik, et al., 2016), it seems that the same or similar mechanisms that lead to the formation of butterfly PADs and penetration into the inner belt of lower energy electrons during a wider range of storms may be able to affect electrons with energies above 1 MeV during stronger storms. While exactly which mechanisms are responsible for these phenomena is still an open question (e.g., Albert et al., 2016; Hua et al., 2019; Li, Ni, et al., 2016), the results shown here do align with previous observations that have been used to argue at lower energies that, during storms, these PADs are being formed at larger L by wave particle interactions (WPIs), potentially by magnetosonic waves, and then moving inwards.

Using instrument simulation and the REPT PHA data, this study is able to come to the following primary conclusions:

1. The energy limit of electron deep penetration ($L < 2$) is at least 1.3 MeV for the storms observed by the Van Allen Probes, which is 30% higher in energy than reported previously. In addition, the REPT PHA data provides a higher-resolution energy spectrum in the inner belt and slot region than the REPT L3 data.
2. The mechanisms that drive the penetration into the inner belt of electrons at 100s keV and at 1 MeV and greater may be similar, because the PADs of ≥1 MeV electron within the slot region and inner belt show similar butterfly PADs to those with energies in the 100s keV. This suggests that the WPIs that drive the formation of these may be similar across a wide energy range.
3. REPT PHA data can be used to produce spin-averaged and PAD flux spectra with a lowered minimum energy and much improved energy resolution compared to the REPT L3 flux.

Because the flux of >1 MeV electrons is low at low L, these conclusions are based on long time averages of the PHA data. Future studies should therefore focus on the behavior of electrons in regions where the fluxes are higher and allow for better time resolution. Additionally, with the new electron channel definitions and analysis complete, the PHA data can be used to look at other phenomena within the radiation belts with improved energy resolution as well.

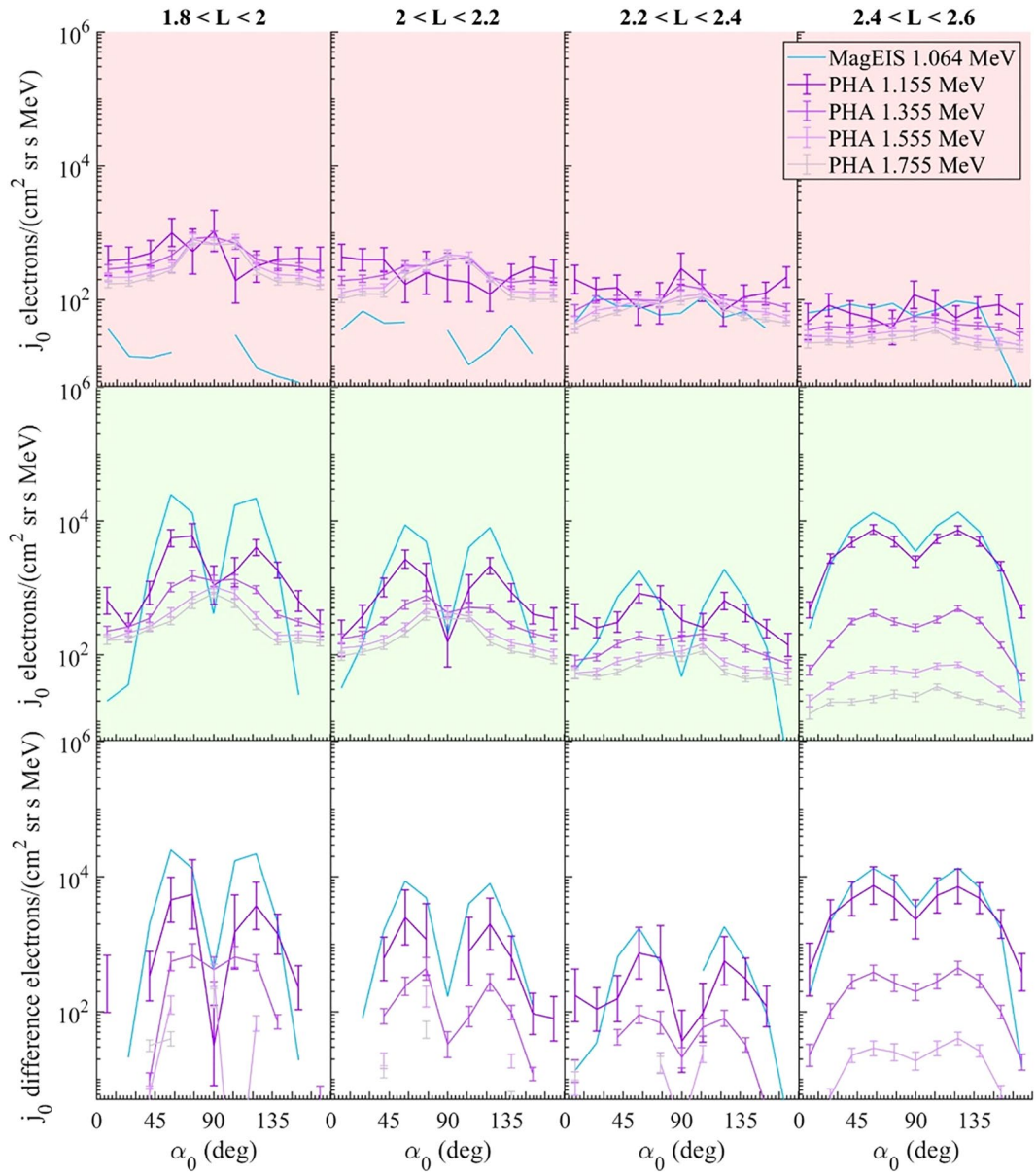

Figure 4. Pitch angle distributions from MagEIS corrected and REPT PHA data for the 2 days before (top row in red) and 2 days after (middle row in green) the September 2017 storm. The bottom row is the difference between the middle row and top row. Fluxes are plotted over equatorial pitch angle. PHA error bars are the uncertainty calculated from the least squares method.

Data Availability Statement

MagEIS and REPT data used in this study are available at https://rbsp-ect.newmexicoconsortium.org/data_pub/ (RBSP ECT, 2013). Geant4 v10.6 was used in this study under an open source license (Geant4, 2023). The Geant4 source code is available at https://geant4.web.cern.ch/.

References

Agostinelli, S., Allison, J., Amako, K., Apostolakis, J., Araujo, H., Arce, P., et al. (2003). Geant4—A simulation toolkit. *Nuclear Instruments and Methods in Physics Research Section A: Accelerators, Spectrometers, Detectors and Associated Equipment*, *506*(3), 250–303. https://doi.org/10.1016/S0168-9002(03)01368-8

Albert, J. M., Starks, M. J., Horne, R. B., Meredith, N. P., & Glauert, S. A. (2016). Quasi-linear simulations of inner radiation belt electron pitch angle and energy distributions. *Geophysical Research Letters*, *43*(6), 2381–2388. https://doi.org/10.1002/2016GL067938

Acknowledgments
REPT and MagEIS data is provided by the Energetic Particle, Composition, and Thermal Plasma Suite (ECT) (Spence et al., 2013). This work could not have been completed without the prior work of the MagEIS and REPT instrument teams who designed the instruments and tools to analyze them and REPTile-2 instrument team who created the methods and tools necessary to perform this reanalysis. The authors additionally thank the REPT team (Baker et al., 2013) and MagEIS team (Blake et al., 2013) for data from their respective instruments. The data used in this study was obtained from https://rbsp-ect.newmexicoconsortium.org/data_pub/. The authors thank Man Hua for useful discussion that contributed to this work. This work was supported by NSF Grant AGS 1834971, NASA Grants 80NSSC18K1276 and 80NSSC21K0583, and by NASA/RBSP-ECT funding through JHU/APL contract 967399 under prime NASA contract NAS5-01072. H. Zhao was supported by NSF Grant AGS 2140934 and NASA Grants 80NSSC22K0356 and 80NSSC21K1041.

Allison, J., Amako, K., Apostolakis, J., Araujo, H., Arce Dubois, P., Asai, M., et al. (2006). Geant4 developments and applications. *IEEE Transactions on Nuclear Science*, *53*(1), 270–278. https://doi.org/10.1109/TNS.2006.869826

Allison, J., Amako, K., Apostolakis, J., Arce, P., Asai, M., Aso, T., et al. (2016). Recent developments in Geant4. *Nuclear Instruments and Methods in Physics Research Section A: Accelerators, Spectrometers, Detectors and Associated Equipment*, *835*, 186–225. https://doi.org/10.1016/j.nima.2016.06.125

Baker, D. N., Jaynes, A. N., Hoxie, V. C., Thorne, R. M., Foster, J. C., Li, X., et al. (2014). An impenetrable barrier to ultrarelativistic electrons in the Van Allen radiation belts. *Nature*, *515*(7528), 531–534. https://doi.org/10.1038/nature13956

Baker, D. N., Kanekal, S. G., Hoxie, V., Li, X., Jaynes, A. N., Zhao, H., et al. (2021). The relativistic electron-proton telescope (REPT) investigation: Design, operational properties, and science highlights. *Space Science Reviews*, *217*(5), 68. https://doi.org/10.1007/s11214-021-00838-3

Baker, D. N., Kanekal, S. G., Hoxie, V. C., Batiste, S., Bolton, M., Li, X., et al. (2013). The relativistic electron-proton telescope (REPT) instrument on board the radiation belt storm Probes (RBSP) spacecraft: Characterization of Earth's radiation belt high-energy particle populations. *Space Science Reviews*, *179*(1), 337–381. https://doi.org/10.1007/s11214-012-9950-9

Bichsel, H. (1988). Straggling in thin silicon detectors. *Reviews of Modern Physics*, *60*(3), 663–699. https://doi.org/10.1103/RevModPhys.60.663

Blake, J. B., Carranza, P. A., Claudepierre, S. G., Clemmons, J. H., Crain, W. R., Dotan, Y., et al. (2013). The magnetic electron Ion spectrometer (MagEIS) instruments aboard the radiation belt storm probes (RBSP) spacecraft. *Space Science Reviews*, *179*(1), 383–421. https://doi.org/10.1007/s11214-013-9991-8

Claudepierre, S. G., O'Brien, T. P., Fennell, J. F., Blake, J. B., Clemmons, J. H., Looper, M. D., et al. (2017). The hidden dynamics of relativistic electrons (0.7–1.5 MeV) in the inner zone and slot region. *Journal of Geophysical Research: Space Physics*, *122*(3), 3127–3144. https://doi.org/10.1002/2016JA023719

Claudepierre, S. G., O'Brien, T. P., Looper, M. D., Blake, J. B., Fennell, J. F., Roeder, J. L., et al. (2019). A revised look at relativistic electrons in the Earth's inner radiation zone and slot region. *Journal of Geophysical Research: Space Physics*, *124*(2), 934–951. https://doi.org/10.1029/2018JA026349

Geant4. (2023). Geant4 version 10.6 [Software]. *The Geant4 toolkit*. Retrieved from https://geant4.web.cern.ch/https://geant4.web.cern.ch/

Hogan, B., Li, X., Zhao, H., Khoo, L., Jaynes, A., Kanekal, S., et al. (2021). Multi-MeV electron dynamics near the inner edge of the outer radiation belt. *Geophysical Research Letters*, *48*(23), e2021GL095455. https://doi.org/10.1029/2021GL095455

Hua, M., Li, W., Ma, Q., Ni, B., Nishimura, Y., Shen, X.-C., & Li, H. (2019). Modeling the electron flux enhancement and butterfly pitch angle distributions on L shells <2.5. *Geophysical Research Letters*, *46*(20), 10967–10976. https://doi.org/10.1029/2019GL084822

Khoo, L.-Y., Li, X., Selesnick, R. S., Schiller, Q., Zhang, K., Zhao, H., et al. (2022). On the challenges of measuring energetic particles in the inner belt: A Geant4 simulation of an energetic particle detector instrument, REPTile-2. *Journal of Geophysical Research: Space Physics*, *127*(4), e2021JA030249. https://doi.org/10.1029/2021JA030249

Li, J., Bortnik, J., Thorne, R. M., Li, W., Ma, Q., Baker, D. N., et al. (2016). Ultrarelativistic electron butterfly distributions created by parallel acceleration due to magnetosonic waves. *Journal of Geophysical Research: Space Physics*, *121*(4), 3212–3222. https://doi.org/10.1002/2016JA022370

Li, J., Ni, B., Ma, Q., Xie, L., Pu, Z., Fu, S., et al. (2016). Formation of energetic electron butterfly distributions by magnetosonic waves via Landau resonance. *Geophysical Research Letters*, *43*(7), 3009–3016. https://doi.org/10.1002/2016GL067853

Li, L. Y., Cao, J. B., Zhou, G. C., & Li, X. (2009). Statistical roles of storms and substorms in changing the entire outer zone relativistic electron population. *Journal of Geophysical Research*, *114*(A12). https://doi.org/10.1029/2009JA014333

Li, L. y., Yang, S. s., Cao, J. b., Yu, J., Luo, X. y., & Blake, J. b. (2019). Effects of solar wind plasma flow and interplanetary magnetic field on the spatial structure of Earth's radiation belts. *Journal of Geophysical Research: Space Physics*, *124*(12), 10332–10344. https://doi.org/10.1029/2019JA027284

Li, L. Y., Yu, J., Cao, J. B., Chen, L. J., Reeves, G. D., & Blake, J. B. (2022). Competitive influences of different plasma waves on the pitch angle distribution of energetic electrons inside and outside plasmasphere. *Geophysical Research Letters*, *49*(1), e2021GL096062. https://doi.org/10.1029/2021GL096062

Li, X., Selesnick, R. S., Baker, D. N., Jaynes, A. N., Kanekal, S. G., Schiller, Q., et al. (2015). Upper limit on the inner radiation belt MeV electron intensity. *Journal of Geophysical Research: Space Physics*, *120*(2), 1215–1228. https://doi.org/10.1002/2014JA020777

Mauk, B. H., Fox, N. J., Kanekal, S. G., Kessel, R. L., Sibeck, D. G., & Ukhorskiy, A. (2013). Science objectives and rationale for the radiation belt storm Probes mission. *Space Science Reviews*, *179*(1), 3–27. https://doi.org/10.1007/s11214-012-9908-y

Ozeke, L. G., Mann, I. R., Murphy, K. R., Jonathan Rae, I., & Milling, D. K. (2014). Analytic expressions for ULF wave radiation belt radial diffusion coefficients. *Journal of Geophysical Research: Space Physics*, *119*(3), 1587–1605. https://doi.org/10.1002/2013JA019204

RBSP ECT. (2013). Science Operations and Data Center [Dataset]. *Radiation Belt Storm Probes Energetic Particle Composition & Thermal Plasma Suite (RBSP ECT)*. Retrieved from hhttps://rbsp-ect.newmexicoconsortium.org/rbsp_ect.php

Roberts, C. S. (1969). Pitch-angle diffusion of electrons in the magnetosphere. *Reviews of Geophysics*, *7*(1–2), 305–337. https://doi.org/10.1029/RG007i001p00305

Selesnick, R. S. (2015). Measurement of inner radiation belt electrons with kinetic energy above 1 MeV. *Journal of Geophysical Research: Space Physics*, *120*(10), 8339–8349. https://doi.org/10.1002/2015JA021387

Selesnick, R. S., Baker, D. N., Jaynes, A. N., Li, X., Kanekal, S. G., Hudson, M. K., & Kress, B. T. (2014). Observations of the inner radiation belt: CRAND and trapped solar protons. *Journal of Geophysical Research: Space Physics*, *119*(8), 6541–6552. https://doi.org/10.1002/2014JA020188

Selesnick, R. S., Baker, D. N., Kanekal, S. G., Hoxie, V. C., & Li, X. (2018). Modeling the proton radiation belt with Van Allen Probes relativistic electron-proton telescope data. *Journal of Geophysical Research: Space Physics*, *123*(1), 685–697. Article 1. https://doi.org/10.1002/2017JA024661

Selesnick, R. S., & Blake, J. B. (2000). On the source location of radiation belt relativistic electrons. *Journal of Geophysical Research*, *105*(A2), 2607–2624. https://doi.org/10.1029/1999JA900445

Spence, H. E., Reeves, G. D., Baker, D. N., Blake, J. B., Bolton, M., Bourdarie, S., et al. (2013). Science goals and overview of the radiation belt storm Probes (RBSP) energetic particle, composition, and thermal plasma (ECT) suite on NASA's Van Allen Probes mission. *Space Science Reviews*, *179*(1), 311–336. https://doi.org/10.1007/s11214-013-0007-5

Tarantola, A. (2005). Inverse problem theory and methods for model parameter estimation. *Society for Industrial and Applied Mathematics*. https://doi.org/10.1137/1.9780898717921

Tarantola, A., & Valette, B. (1982). Generalized nonlinear inverse problems solved using the least squares criterion. *Reviews of Geophysics*, *20*(2), 219–232. https://doi.org/10.1029/RG020i002p00219

Yu, J., Li, L. Y., Cao, J. B., Reeves, G. D., Baker, D. N., & Spence, H. (2016). The influences of solar wind pressure and interplanetary magnetic field on global magnetic field and outer radiation belt electrons. *Geophysical Research Letters*, *43*(14), 7319–7327. https://doi.org/10.1002/2016GL069029

Zhao, H., Califf, S. T., Goyal, R., Li, X., Gkioulidou, M., Manweiler, J. W., & Krantz, S. (2023). Statistical analysis of the differential deep penetration of energetic electrons and protons into the low L region (L < 4). *Journal of Geophysical Research: Space Physics*, *128*(4), e2022JA031125. https://doi.org/10.1029/2022JA031125

Zhao, H., Friedel, R. H. W., Chen, Y., Reeves, G. D., Baker, D. N., Li, X., et al. (2018). An empirical model of radiation belt electron pitch angle distributions based on Van Allen Probes measurements. *Journal of Geophysical Research: Space Physics*, *123*(5), 3493–3511. https://doi.org/10.1029/2018JA025277

Zhao, H., Li, X., Blake, J. B., Fennell, J. F., Claudepierre, S. G., Baker, D. N., et al. (2014a). Characteristics of pitch angle distributions of hundreds of keV electrons in the slot region and inner radiation belt. *Journal of Geophysical Research: Space Physics*, *119*(12), 9543–9557. https://doi.org/10.1002/2014JA020386

Zhao, H., Li, X., Blake, J. B., Fennell, J. F., Claudepierre, S. G., Baker, D. N., et al. (2014b). Peculiar pitch angle distribution of relativistic electrons in the inner radiation belt and slot region. *Geophysical Research Letters*, *41*(7), 2250–2257. https://doi.org/10.1002/2014GL059725

Zheng, Y., Lui, A. T. Y., Li, X., & Fok, M.-C. (2006). Characteristics of 2–6 MeV electrons in the slot region and inner radiation belt. *Journal of Geophysical Research*, *111*(A10), A10204. https://doi.org/10.1029/2006JA011748